J Radioanal Nucl Chem (2013) 296:541–549
DOI 10.1007/s10967-012-2061-y

Atomic layer deposition α-Al_2O_3 diffusion barriers to eliminate the memory effect in beta-gamma radioxenon detectors

W. K. Warburton · Wolfgang Hennig · Jacob A. Bertrand · Steven M. George · Steven Biegalski

Received: 19 July 2012 / Published online: 21 August 2012

Abstract Well designed scintillator detectors, including such examples as ARSA, SAUNA, and XIA's "PhosWatch", can readily achieve the state of the art radioxenon detection limits required for nuclear explosion monitoring. They are also reliable, robust detectors that do not require cryogenic cooling for operation. All three employ the principle of beta-gamma coincidence detection to reduce background counting rates, using a BC-404 plastic scintillator to detect the betas and a CsI or NaI scintillator to detect the gamma-rays. As a consequence of this commonality of design, all three also display a "memory effect" arising from the diffusion of Xe into BC-404. Thus, when one sample is pumped out of the detector, a fraction remains behind, embedded in the BC-404, where it artificially raises the signal counting rate for the next sample. While this is not a fatal flaw in scintillator detectors, developing a method to eliminate the memory effect would significantly enhance their utility. This paper reports efforts to develop thin, amorphous Al_2O_3 films, deposited by atomic layer deposition (ALD) to act as diffusion barriers on the BC-404 surfaces exposed to radioxenon. Using radon as a convenient substitute for Xe, film thicknesses between 2 and 10 nm were originally investigated and found to show a memory effect to varying degrees. A second set of 20 and 30 nm films was then produced, which appeared to completely eliminate the radon memory effect, but, when consequentially tested with radioxenon, were found to exhibit xenon memory effects that were approximately half of the effect found on uncoated BC-404. We draw two conclusions from this result. The first is that it will be necessary to develop an improved method for depositing thicker ALD Al_2O_3 films at lower temperatures while still retaining high film quality. The second is that, since xenon is required to test for the xenon memory effect, we need a test method that does not require xenon radio-isotopes in order to facilitate screening large numbers of samples.

Keywords Radioxenon detection · Memory effect · Vapor barrier · Al_2O_3 · Atomic layer deposition · ALD · Beta-gamma detector

W. K. Warburton (✉) · W. Hennig
XIA LLC, Hayward, CA 94544, USA
e-mail: bill@xia.com

J. A. Bertrand · S. M. George
University of Colorado, Boulder, CO 80309, USA

S. Biegalski
The University of Texas at Austin, Austin, TX 78712, USA

Introduction

XIA, supported by the DOE's SBIR program, developed a "PhosWatch" phoswich radioxenon detector [1] intended for use in verification operations by the Comprehensive Nuclear-Test-Ban Treaty Organization (CTBTO) [2]. The PhosWatch, like the SAUNA [3] and ARSA [4] detectors, is a beta-gamma coincidence detector that uses a fast plastic scintillator BC-404 sample cell to detect beta particles and conversion electrons. It differs from these detectors in that the BC-404 is formed as a spherical shell embedded in and optically coupled to a cylinder of CsI(Tl) that is read out by a single PMT, and beta-gamma coincidences are detected by pulse shape analysis of the single PMT output, rather than by timing analysis of multiple PMT outputs. This approach has been shown to achieve minimum detection limits similar to SAUNA and ARSA, but is cheaper, less complex and easier to operate and keep calibrated in the field [2].

However, because the PhosWatch shares the same BC-404 sample cell material with the SAUNA and ARSA detectors, it also suffers from the same radioxenon memory effect, [4, 5] which is attributed to the diffusion of radioxenon into the BC-404 plastic (polyvinyltoluene) during the 24 h counting period. Thus, when a new sample is introduced, some fraction of the previous sample remains, embedded in the BC-404 and contributing to the new count rate. In the present CTBTO protocol, some attempt to mitigate this effect is made by taking a background count between samples [6, 7] but there is currently an ongoing informal discussion in the community about how to do this correctly, since the sample cell is sealed during the background count but then pumped again before the new sample is introduced, thereby removing an unknown fraction of the memory gas that diffuses back into the sample volume during the measurement. Therefore it would be far preferable to instead develop means for eliminating the memory effect.

This paper reports on our recent efforts to develop a method to eliminate the memory effect by coating the inside of the BC-404 sample cell with a thin vapor barrier made of amorphous aluminum oxide (α-Al_2O_3) deposited by atomic layer deposition (ALD) [8]. Al_2O_3 was chosen because: first, it is a dense inorganic material which should not have large internal free volumes to allow the diffusion of Xe atoms; second, it is transparent in thin sections and so will not interfere with light collection within the PhosWatch geometry; and third, it is chemically very inert, which is desirable for the long term stability of the treatment. The amorphous form was chosen because grain boundaries are known fast diffusion channels and are extremely numerous in thin crystalline films, which are almost invariably polycrystalline with grain boundary separations commensurate with the film thickness. We selected ALD to deposit the films both because the technique can operate at relatively low temperatures while producing α-Al_2O_3 films of high density and perfection [9] that have been used as vapor barriers for several gases [10] and because it has also been shown to be capable of depositing α-Al_2O_3 films that adhere well to a variety of polymers [11].

In a previous report [12] we described our experimental plan and methods. First, we used ALD equipment at the University of Colorado, Boulder to deposit α-Al_2O_3 films on a series of BC-404 samples, varying both film thickness and deposition temperature. Second, we built and tested an apparatus for dosing BC-404 with radon. We selected radon as a substitute for xenon in our initial research because: (1) it is also a noble gas whose atomic radius is only slightly larger than xenon's (120 vs 108 pm) [13] and so should diffuse similarly; (2) it is much easier to obtain commercially than radioxenon, which greatly simplifies making an extended series of measurements; and, (3) it also has a reported memory effect in BC-404 [4]. Third, we developed a phoswich detector that would allow us to carry out both singles and coincidence counting for either xenon or radon, using the same pulse shape analysis method as for our PhosWatch detector. Fourth, we conducted initial measurements to show that our methods were working successfully.

Our major objectives in continuing the research were therefore to: conduct measurements to study the memory effect as a function of film thickness and growth temperature; identify a film growth process that would produce a film that eliminated the radon memory effect; and test films grown using this process to measure their xenon memory effect.

Research accomplished

Experimental methods

Radon measurement

Our experimental methods have been described in detail [12] and will only be summarized briefly here. First, we constructed a specialized CsI(Tl)-BC-404 phoswich detector that would allow the BC-404 to be exposed to either radon or radioxenon in situ. This was accomplished by attaching the BC-404 to an aluminum dosing cap (see Fig. 1), placing the BC-404 in contact with one window of a two window container housing a CsI(Tl) crystal, and connecting the other window to a PMT, which was thereby optically coupled to both the CsI(Tl) crystal and to the BC-404. The entire assembly was enclosed in a light-tight housing. An external pumping/dosing system allowed the face of the BC-404 away from the CsI(Tl) crystal to be exposed to either radon or radioxenon for arbitrary periods of time. The PMT signal was processed using a Pixie-4 PXI module from XIA [14] and the same Igor software and algorithms developed at XIA to process PhosWatch signals [1]. All counting was done in a small lead cave whose background counting rate was about 5 cps with no sign of radon contamination.

Figure 2 presents a typical radon "coincidence" spectrum produced by our equipment. The y-axis shows the "gamma-ray energy" that the pulse shape analysis software detects in the CsI(Tl) crystal, while the x axis shows the "electron energy" that it detects in the BC-404. Both axes have been approximately calibrated using the peak and Compton scattering created by 662 keV gamma-rays from a ^{137}Cs source. In looking at Fig. 2, it is important to remember that these energies are inferred by an analysis method that assumes that the PMT pulse shape is composed

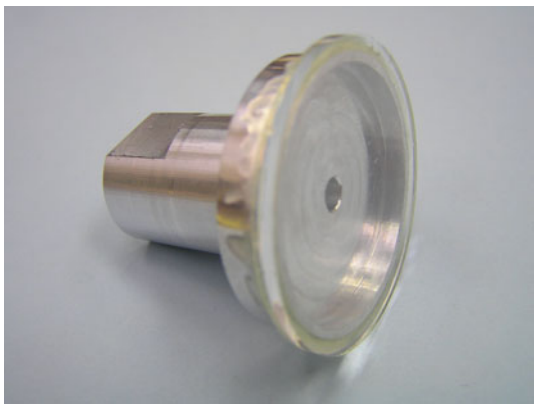

Fig. 1 BC-404 with its Al dosing cap

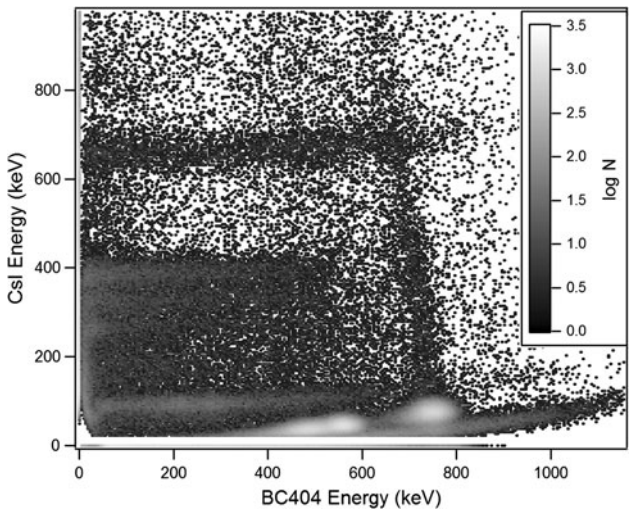

Fig. 2 Typical Rn spectrum collected by the test jig

of a super-position of two shapes, one generated by an electron stopping in BC-404 and one generated by a gamma-ray being absorbed in CsI(Tl). When the actual pulse shape is generated by a different mechanism, specifically by the absorption of an alpha particle in BC-404, the program decomposes it into these two shape terms and "finds" a small "gamma-ray" term. Thus, even though the alpha particles are not actually in coincidence with anything, they still show up in a 2-D coincidence plot such as Fig. 2. Further, because of quenching along the alpha particle's track within the BC-404, the reported "electron" energy is smaller by almost an order of magnitude than the alpha particle's actual energy. Thus the three bright spots at the bottom of Fig. 2 are alpha particles emitted by radon and its daughters: ^{222}Rn (at ~430 keV), ^{218}Po (at ~500 keV), and ^{214}Po (at ~670 keV), whose actual energies are 5.49, 6.00, and 7.69 MeV, respectively. The horizontal lines in Fig. 2 below 100 keV and between 200 and 400 keV come from the ^{214}Pb daughter isotope emitting K X-rays and gamma-rays in coincidence with either a beta or an EC electron. The horizontal line at about 600 keV is similarly from ^{214}Bi's 609 keV gamma in coincidence with a beta. At this time we do not have a clear explanation for either the nearly vertical line that appears to terminate on the ^{214}Po alpha peak or the bright line underlying the alpha particle peaks. We are not unduly concerned about these features since the device is not intended to function as a high quality spectrometer and needs only be sensitive to the presence of radon to be useful.

Because the 2-D radon spectrum is complex, we did not attempt to isolate sections of it due solely to ^{222}Rn and instead chose to record total counts/sec, depending upon the fact that ^{222}Rn reaches secular equilibrium with all of its daughters above ^{210}Pb in less than 2.5 h. Thus, in our measurements, we exposed the BC-404 to radon for about 24 h, while counting, and then evacuated the sample volume. We continued to count for another 24–72 h while pumping continuously. By developing a model, further described below, of the expected counting rate throughout the complete dosing-pumping cycle we showed that we could extract the xenon memory effect by fitting the curve during the pumping phase using a two exponential fitting function. Of these two exponentials, the shorter one describes the decay of the non-volatile Rn daughters left in the sample cell after the Rn is evacuated, while the longer one corresponds, approximately, to the decay time of any Rn remaining trapped in the sample. The amplitude of the second term therefore reflects the amount of memory effect in the sample being analyzed.

Sample preparation

Our sample preparation methods have also been described earlier [12]. Briefly, disks of BC-404 were obtained from St. Gobain and coated with different thicknesses of α-Al_2O_3 films at several deposition temperatures using existing ALD equipment at the Departments of Chemistry and Chemical Engineering at the University of Colorado, Boulder (see George, [8] and references therein). To avoid sample deformation and bubbling, all samples were outgassed overnight at 70 °C while supported on polished Si wafers. The film thicknesses and deposition temperatures are shown in Table 1. As shown, the samples were prepared in two batches, one with thicknesses between 2 and 10 nm and a second with thicknesses of 20 and 30 nm after the first batch proved incapable of completely blocking the Rn memory effect, as we discuss below.

All samples were produced in a flow reactor by alternately dosing the sample with TMA (tri-methyl-aluminum: $Al(CH_3)_3$) and water vapor (H_2O) with purge times in between to completely remove each reactant before introducing the next. The standard conditions are: 100 sccm of Ar carrier gas at a base pressure of about 1 Torr; TMA

Table 1 Sample deposition schedule

Temperature (°C)	Thickness (nm)	Quantity
First sample set		
75	7	4
85	7	4
100	2	4
100	5	4
100	7	4
100	10	4
Second sample set		
100	20	4
100	30	4

dose time of 1.0 s; TMA purge time of 120 s for sample thicknesses of 10 nm or less, 90 s for thicker films; water dose time of 0.5 s; water purge times same as TMA purge times. The pressure rise during dosing was 400–500 m Torr. Dosing times had been previously established using quartz crystal microbalances (QCM's), as was the deposition rate of 0.128 nm/cycle. The number of deposition cycles was established by dividing the desired thickness by the known deposition rate/cycle. All of the samples were deposited above BC-404's 70 °C softening point [15] and minor amounts of sample sagging were observed, particularly for the longer deposition times, which approach 8 h for the 30 nm sample. Some of the thicker sample also showed areas with some "frostiness" which we presume to come from additional Al_2O_3 deposition by chemical vapor deposition (CVD) arising from incomplete H_2O removal during the shorter H_2O purge times. Only areas without visible frostiness were selected for memory effect testing. But the presence of CVD suggests that these samples may not have been as atomically perfect as the best ALD films that can be produced.

Radioxenon measurements

Radioxenon memory effect tests were performed at the University of Texas at Austin (UTA) in two ways. The first was the same as the radon method described above, but instead exposing the BC-404 to radioxenon. In the second method, the BC-404 sample and its aluminum holder were removed from the phoswich counting assembly and filled directly with radioxenon and held for 24 h. The sample was then placed on top of an HPGe gamma-ray spectrometer and its spectrum collected and the counting rate in the 80 keV ^{133}Xe line recorded. The sample was then evacuated for 24 h, resealed, replaced in exactly the same position on the gamma-ray spectrometer and the counting rate in the 80 keV ^{133}Xe line recorded as second time. The ratio of the two was used directly as an upper bound measurement of the memory effect without correcting for ^{133}Xe's 5 day half life.

Experimental results and analysis

The radon 1-D finite element dosing model

At a general conceptual level, the interaction of radon with a BC-404 sample coated with a diffusion barrier is fairly straightforward. During dosing, two regions containing radon and its daughters are visible to the counting system: the volume over the sample and the sample volume itself, with the two separated by the diffusion barrier. When the radon is first introduced, there are no daughters and, as time goes on, secular equilibrium is eventually established. Because the radon is mobile and the daughters are not, the latter remain where they are generated, while the radon penetrates the diffusion barrier and moves into the BC-404 at a rate governed by its diffusivity. When pumping begins, all radon is removed from the volume over the sample. Some of the radon within the sample now begins to diffuse out through the diffusion barrier, to be pumped away, while the remainder continues to diffuse further into the BC-404 bulk. Any daughters created during the dosing process continue to be counted until they decay away, while the radon within the BC-404 continues to generate new daughter products.

Because this process is controlled by several kinetic coefficients, including (1) the coefficients for Rn sticking to and evaporating from the diffusion barrier; (2) the radon diffusivity across the barrier; and, (3) the diffusivity of radon within the BC-404, it is much more difficult to predict exactly what will occur in any given circumstance. We therefore developed a 1-D finite element model to explore the possibilities, assuming that the radon in the sample was always well below its saturation density. The model includes both diffusion and radioactive decay.

The "elements" in the model were: (1) the volume over the BC-404; (2) the sample surface; (3) a "barrier" layer with Rn diffusivity kBar; and, (4) 100 layers of BC-404 with Rn diffusivity kDiff. The proportionality constants for the Rn depositing on the surface and evaporating from it were kDep and kEvap. Standard finite difference equations were then written to describe the motion of the Rn out of the gas and through the sample. At each time step the decay of Rn and each of its daughters was calculated using their known lifetimes, both to adjust the concentration profiles appropriately and to find the total observable counting rate. The model is heuristic in the sense that the diffusion coefficients are all treated as unknowns and adjusted to produce output counting curves that mimick those actually observed.

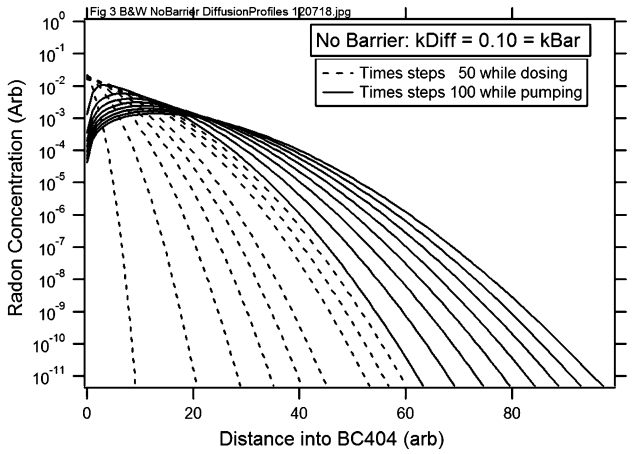

Fig. 3 Rn concentration profiles in BC-404 as a function of time with no surface absorption barrier

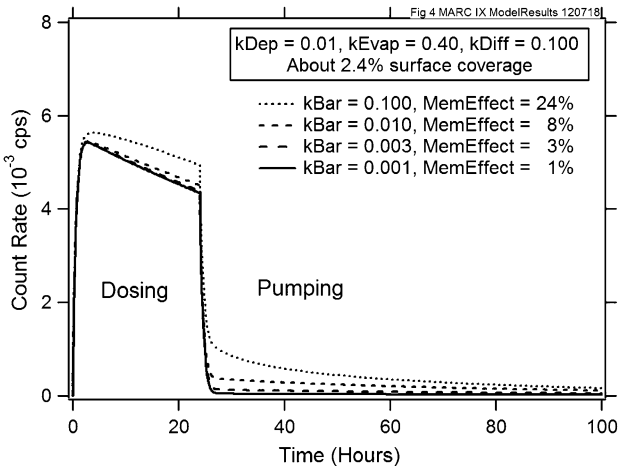

Fig. 4 Modeled count rate versus time and barrier value

Figure 3 shows concentration profiles in uncoated BC-404 during dosing, which are typical of diffusion with a pinned surface concentration (dashed) and after pumping starts at 24 h (solid). In interpreting these curves it is important to recall that diffusion moves material in the direction of decreasing concentration. Thus, during dosing (dashed) the Rn moves only into the BC-404. During pumping (solid) however, Rn to the left of the maximum moves toward the surface to escape the BC-404 and be pumped away, while the material to the right of the maximum, which is a large fraction of the total, continues to diffuse inward. This is an important result: all the Rn (or Xe) cannot be removed by pumping since the interior is also technically a Rn vacuum and any given atom is as likely to move toward the interior as toward the surface. Because we are pumping, any Rn reaching the surface is removed, which shortens the Rn activity's apparent decay time from its natural half life.

Figure 4 shows the time dependence of total activity with barriers ranging from none (kBar = kDiff) to one with kBar = 0.01 × kDiff. These curves during pumping can be fit well with a double exponential, the first one modeling the decay of the Rn daughters, the second modeling the Rn leaving the BC-404 by both diffusion and radioactive decay. The first time constant is typically of order 1 h, the second of order 1–3 days. Examining the decay curves as a function of increasing diffusion barrier reveals two results of interest: first, as expected, the memory effect is reduced as Rn is prevented from entering the BC-404; and, second, the post-removal decay time increases because better barriers also trap Rn inside the BC-404 where its concentration can be reduced only by radioactive decay with its natural 3.82 day half life.

In this work we compute the "memory effect" as the ratio of the slow term amplitude to the sum of the two amplitudes. This sum represents the total activity in the cell and sample the instant before the gaseous Rn charge is pumped away. This definition overestimates the amount that would be present after a typical 24 h pump, but we use it both because it is well defined in this analysis and because it sets an upper bound on the effect we will be trying to minimize. Figure 4 also shows that, when the barrier is porous (memory effect 24 %) the reduction in memory effect with barrier diffusivity is sub-linear: decreasing kBar by a factor of 10, from 0.100 to 0.010 only reduces the memory effect by a factor of 3. However, as the barrier improves, the memory effect becomes more nearly linear in kBar, reducing from 3 to 1 % as kBar decreases from 0.003 to 0.001. These results suggest that we will have to produce a barrier film whose Xe diffusivity is of order 1,000 times lower than the diffusivity of Xe in BC-404 in order for it to be effective.

Radon measurements on the first set of BC-404 samples

The first set of samples was intended to explore the α-Al_2O_3 layer's ability to block Rn diffusion as a function of its thickness and deposition temperature. Since our experience has been that α-Al_2O_3 layers of a few nanometers effectively block water diffusion [16] and water molecules are smaller in size than either Xe or Rn atoms, we began, as shown in Table 1, with a set of film thicknesses between 2 and 10 nm. In selecting an optimum growth temperature, we considered both the 70 °C softening point of BC-404 and the observation that α-Al_2O_3 film densities increase with increasing deposition temperature [9]. Since we expect the film's barrier efficiency to increase as its free volume drops (density rises), we selected temperatures slightly above the softening point, hoping that excess deformation would not occur during deposition. Because this was an exploratory study, we did

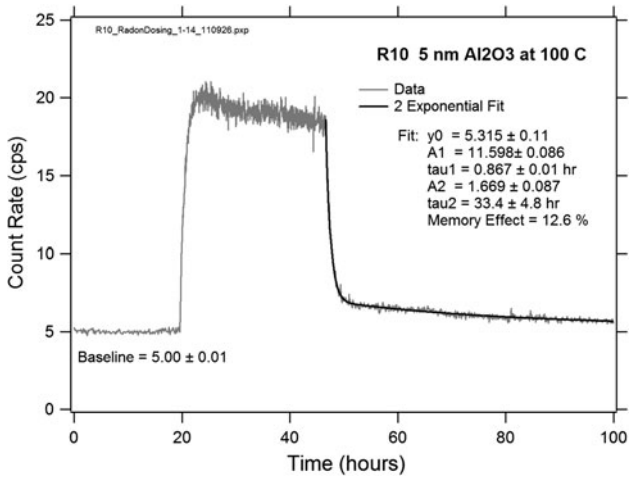

Fig. 5 A Rn dosing curve with a 2-exponential fit

not undertake a detailed study to determine optimum dosing and purging times, but instead used values in the range that produced good water barrier films on other plastics [9, 10].

As described in the experimental section, each tested sample resulted in a record of total count versus time over a period that included a 24 h background count, a 24 h Rn exposure, and a count of 24–72 h under vacuum. Figure 5 shows a typical curve (gray), taken on a 5 nm film that was deposited at 100 °C. The fit parameters of the two exponential fit (solid) are also shown, together with the calculated memory effect ME in percent:

$$\mathrm{ME} = 100\,\frac{A2}{A1 + A2}. \quad (1)$$

Note that, because ME is found from a fit to data, the value of $A2$ can be negative, even though such a result is not physically possible. To obtain this measured value, the real value of $A2$ would have to be small compared to fluctuations in the background rate.

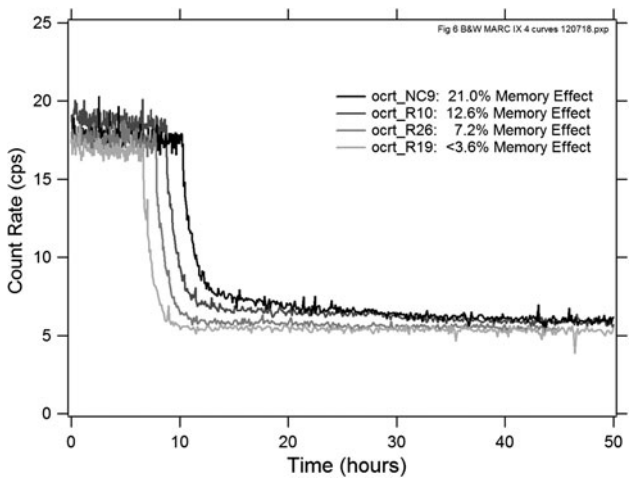

Fig. 6 Four dosing curves showing a range of memory effect values

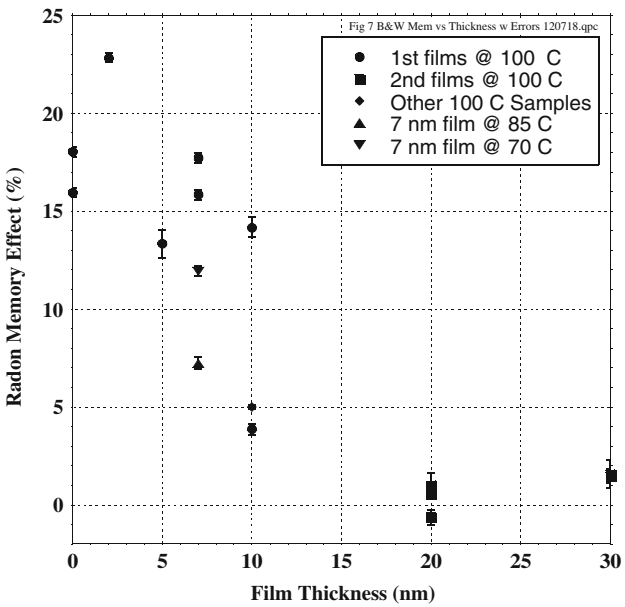

Fig. 7 Measured memory effect values

Figure 6 shows the dosing and decay portions of curves from four samples that illustrate the range of memory effects that we measured on these samples. The observed memory effects range for about 3–21 %, where the largest value is for an uncoated sample and the smallest for a 10 nm film. In the latter case the second exponential region was sufficiently flat that it could not be fit using both $A2$ and Tau2 as independent parameters. When Tau2 was forced to the half life of Rn, then values for $A2$ between 3 and 4 % were found, depending on the precise fitting range selected.

Figure 7 shows the values of the memory effect that we obtained from this set of samples, which are all the values with film thicknesses of 10 nm or less. It is worth noting that these values cannot be directly compared to values seen for radioxenon. This is primarily because a measured memory effect value depends not only on the solubility and diffusivity of the radio-isotope in BC-404 but also on the sample volume and surface area. Thus, if one starts with N atoms and D of them diffuse into the BC-404, the memory effect will be D/N. Here D varies with the sample area, BC-404 diffusivity and solubility, and barrier efficiency, while N varies with sample cell volume and pressure. Because, in our experiments, we keep everything constant except the barrier efficiency, we can directly compare our results to the uncoated case to obtain barrier efficiencies. But we cannot make quantitative comparisons to experiments made under other conditions. The sole exception to this identical treatment rule was the 2 nm sample, which was dosed for 48 h instead of the usual 24 h and, as a result, shows a distinctly larger memory effect. The remainder of the samples that were nominally dosed for

24 h were all actually dosed for this time with an accuracy of about 1 h. The two uncoated samples were dosed for 89,100 and 91,200 s, a difference of 2.4 %, which is not sufficient to account for their 2 % memory effect difference if an extra 24 h (86,400 s) raises the memory effect of the 2 nm sample by perhaps 6 %.

All the data points in Fig. 7 have error bars obtained from the fitting parameters, although in some cases they are smaller than the point sizes. Looking at the data, then, we can conclude that, while there is a general trend to smaller memory effect values as the film thickness increases, the measurements have other sources of error that are large compared to the fitting errors. Some of this fluctuation arises from the measurement technique itself, primarily from fluctuations in background counting rate, but it is not large enough to account for the discrepancies seen. In particular, we measured several samples twice and obtained answers that typically agreed within about 0.5 %.

As an example of these discrepancies, consider the values at 7 nm: the films deposited at higher temperatures, which should be denser, actually have the largest memory effect. The trend for all four samples is exactly opposite from what one would physically expect. Similarly, the two measurements at 10 nm are widely separated. The diamond point at 10 nm is the same sample that produced the 4 % memory effect, but with 2″ of Teflon tape introduced into the sample volume to see if the small amounts of pipe tape in the system would contribute to our measured values. But this value reproduced within 1 % (5 % vs 4 %), showing that this sample is indeed significantly different from the one with a 14 % memory effect.

Radon measurements on the second set of BC-404 samples

One possible explanation is that α-Al_2O_3 films are known not to reliably nucleate on certain plastic substrates [11] and may take up to 10 min before they begin growing at a rate that is no longer influenced by the substrate material. To test this hypothesis, we deposited two more sets of samples at 100 °C of thicknesses 20 and 30 nm. The dosing curves for three of the 20 nm samples are shown in Fig. 8. In all three cases, once the Rn was pumped out, the only activity remaining was the decay of Rn daughters in the sample cell. The curves could be fit to two exponentials only by fixing the decay time of the slow component to the half live of Rn. The resulting slow component amplitudes were small and, in one case, negative, suggesting that the true value is zero with a standard deviation of less than 1 % determined by fluctuations in the background counting rate. The values for the two 30 nm samples were also quite small, at the 1.5 % level. These five points are the square points in Fig. 7. It therefore appears that either a 20 or

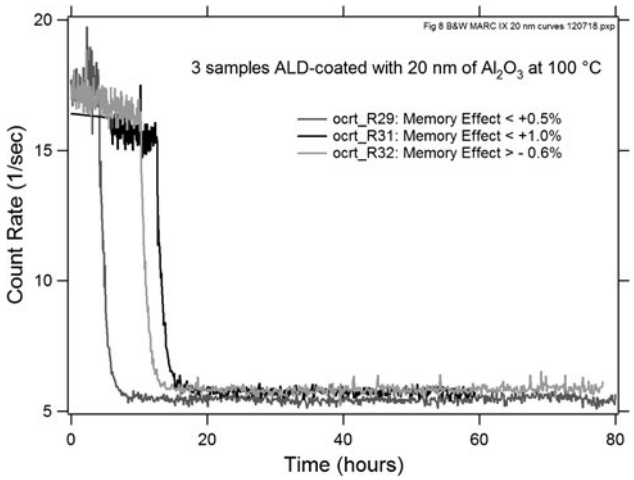

Fig. 8 Rn dosing curves for three 20 nm films, showing no memory effect

30 nm α-Al_2O_3 film makes a Rn barrier that reduces the memory effect by a minimum factor of at least 10.

Radioxenon measurements on the 30 nm ALD films

Having produced films that provided a good Rn barrier, we proceeded to test them with radioxenon produced by irradiating natural Xe in a reactor at The UTA. The results, however, were dis-appointing. We first tested a 20 nm film, sample R32 (see Fig. 8), with the only changes in our experimental measurement program being, first, the substitution of radioxenon for Rn, and, second, the addition of a quick release valve to the fill tube on our phoswich detector because the Xe gas handling equipment was in a different room from the counting laboratory at UTA.

Figure 9 shows a the first radioxenon spectrum, which demonstrates that, while still uncalibrated, our phoswich detector is working correctly. The initial counting rate was

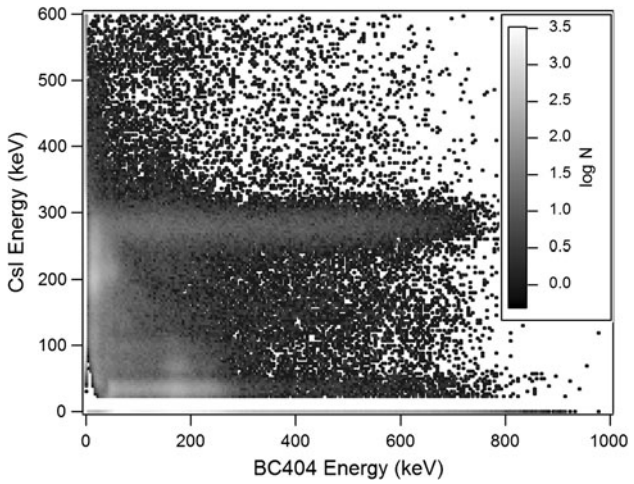

Fig. 9 2-D spectrum from irradiated natural Xe

fairly high, at about 5,000 cps. The Xe and Cs Kα X-ray lines near 30 keV are clearly visible and show peaks from conversion electrons captured in the BC-404.

We recorded the counting rate for 19.6 h, by which time it had dropped to about 87 cps, a reduction factor of almost 60. We then pumped out the Xe, which dropped the counting rate to about 16 cps, which would correspond to a memory effect of about 18 %. We cannot, however, account for the factor of 60 reduction in count rate over 24 h without invoking a leak in the system because the reduction factor of the shortest half life Xe isotope (^{135g}Xe—9.14 h) is only 8.5 over 19.6 h. We therefore do not regard this memory effect measurement as reliable since, in the presence of a leak it is easier for free Xe to escape from the cell volume than it is for absorbed Xe to escape from the BC-404 sample.

We therefore measured a 30 nm film using the second method for measuring the radioxenon memory effect described above. 24 h after filling the cell with radioxenon, it took 299.3 s to obtain 12,480 ± 119 counts in the 81 keV ^{133}Xe peak (41.70 ± 0.40 cps). The radioxenon was then removed with four pump and flush cycles and the cell counted again, taking 14,400 s to obtain 16,323 ± 138 counts in the 81 keV ^{133}Xe peak (1.13 ± 0.01 cps). The memory effect is the ratio of the two counting rates and is 2.70 ± 0.0035 %, where we have not made the small correction for the 5.25 day ^{133}Xe half life. Since the Xe memory effect is typically reported to be about 5 %, [4, 7, 17] the 30 nm α-Al_2O_3 coating reduces it by about 50 %. This is in agreement with the absolute memory effect results reported by Bläckberg et al. [17].

Discussion

Rn and Xe clearly behave quite differently in relation both to BC-404 and to the α-Al_2O_3 ALD films with which we are attempting to reduce the memory effect. Thus, while Rn has a factor of 4 larger memory effect than Xe in BC-404, 20 % compared to 5 %, Xe clearly has a much higher diffusivity through α-Al_2O_3, considering that a 30 nm film blocks the one nearly completely but barely hinders the other. Several factors may be contributing here.

First, under the growth conditions that produced our ALD α-Al_2O_3 films, it is known that the film density increases with increasing deposition temperature, from 2.5 g/cm^3 at 35 °C to 3.0 g/cm^3 at 177 °C, being about 2.7 g/cm^3 at 100 °C. This compares to 3.97 g/cm^3 for crystalline Al_2O_3 (corundum). Since interstitial diffusivity rates are controlled by the passage of atoms through the small holes between the interstices, they are quite sensitive to the dimension of the atom compared to the dimension of the connecting holes. Thus, if the holes are slightly smaller than the diameter of one diffusing species and slightly larger than the diameter of another, then the first may move quite freely while the second may be essentially blocked. In addition, it is known that growing ALD α-Al_2O_3 films at lower temperatures incorporates varying amounts of hydrogen, [9] which might also influence diffusion rates by modifying the growth structure through bond termination.

Second, in both this work and that of Bläckberg et al. [17] there is significant sample to sample variation that remains unexplained. Bläckberg et al. suggests that this might be due to variations in surface roughness, which is not currently a controlled or varied parameter. However, in our research we have noted that there appears to be some kind of volatile solvent in the BC-404 samples that cause bubbling when the samples were coated at 100 °C or above and which we removed by baking the samples overnight at 70 °C prior to coating. Our working assumption, which needs to be verified, is that this is water. If true, then this provides an H_2O reservoir to chemically react with TMA during the TMA exposures in the ALD cycle. This process would produce CVD α-Al_2O_3, which lacks the film perfection of ALD grown oxide. Differing amounts of water, sample to sample could then produce variable results, independent of surface roughness variations.

Third, the growth of α-Al_2O_3 by ALD as a function of dose times, purge times and temperature on BC-404 has not been carefully studied or optimized as it has been in certain cases [11]. In particular, the purge times to adequately remove water vapor have not been demonstrated, while it is known that inadequate removal of water vapor can be deleterious to film quality. It is thus likely that the currently grown films are not of optimal quality.

Conclusions and recommendations

In summary, we developed a method for testing the memory effect of Rn on BC-404 samples coated with α-Al_2O_3 by ALD, using Rn as a substitute for Xe due to the difficulties in making large numbers of measurements without ready access to either a reactor or a commercial source of radioxenon. We found that coatings of 20 or 30 nm, deposited at 100 °C effectively blocked the memory effect for Rn, but only reduced it by half for Xe. In the future, then, the films will have to be tested using Xe. Because the pressures involved are large, it may be possible to make useful measurements using natural Xe and accurate pressure gages, reserving tests with radio-isotopes for only the best samples. The uncertainties we and others have found in memory effect measurements are currently not well understood, which suggests that it would be worthwhile to carry out more fundamental studies on the ALD process used to produce the films in order to obtain a

better understanding of the relationship between growth parameters and the measures of film quality, such as density, that may be important to its role as a diffusion barrier. Methods for reducing purge times while avoiding CVD during low temperature ALD would be particularly useful since significant sample deformation occurred during even the shorter depositions at 100 °C and it would be preferable to be able to deposit the Al_2O_3 films at temperatures below BC-404's softening point without simultaneously reducing film density.

Finally, the view that Xe diffusion rates in both BC-404 and the Al_2O_3 films are controlled by free volume suggests a different line of research that may be interesting to pursue, the use of crystalline fast organic scintillator as a replacement for BC-404. Recent work has shown that such materials as Stilbene, which is an fast organic scintillator with a much higher light output that BC-404, can be grown in large single crystals [18]. Being crystalline, these materials do not possess the large free volumes found in cast plastics like BC-404, which are thought to form fast diffusion channels for Xe, and therefore, conceptually, should have significantly reduced memory effects.

References

1. Hennig W, Warburton WK, McIntyre JI (2006) IEEE Trans Nucl Sci 53:620
2. Hennig W, Warburton WK, Fallu-Labruyere A, Sabourov K, Cooper MW, McIntyre JI, Gleyzer A, Bean M, Korpach EP, Ungar K, Zhang W, Mekarski P (2009) J Radioanal Nucl Chem 282:681
3. Ringbom AT, Larson T, Axelson A, Elmgren K, Johansson C (2003) Nucl Instr Meth Phys Res A 508:542
4. McIntyre JI, Abel KH, Bowyer TW, Hayes JC, Heimbigner TR, Panisko ME, Reeder PL, Thompson RC, Radioan J (2001) Nucl Chem 248:629
5. Seifert CE, McIntyre JI, Antolick KC, Carman AL, Cooper MW, Hayes JC, Heimbigner TP, Hubbard CW, Litke KE, Ripplinger MD, Suarez R (2006) In: Proceedings of 27th seismic research reviews: ground-based nuclear explosion monitoring technologies, LA-UR-05-6507, vol II, pp 804–814
6. Kalinowski MB, Becker A, Saey PRJ, Tuma MP, Wotowa G (2008) Complexity 14:89
7. Auer M, Kumberg T, Sartorius H, Wernsperger B, Schlosser C (2010) Pure Appl Geophys 167:471
8. George SM (2010) Chem Rev 110:113
9. Groner MD, Fabreguette FH, Elam JW, George SM (2004) Chem Mater 16:639
10. Groner MD, George SM, McLean RS, Carcia PF (2006) Appl Phys Lett 88:051907
11. Wilson CA, Grubbs RK, George SM (2005) Chem Mater 17:5625
12. Warburton WK, Asztalos SJ, Hennig W (2011) In Proceedings of 2011 monitoring research review: ground-based nuclear explosion monitoring technologies, LA-UR-11-4823, vol II, pp 731–740
13. Clementi E, Raimondi DL, Reinhardt WP (1967) J Chem Phys 47:1300
14. Hennig W, Chu YX, Tan H, Fallu-Labruyere A, Warburton WK, Grzywacz R (2007) Nucl Instr Meth Phys Res B 263:175
15. Saint-Gobain Data Sheet. BC-400, BC-404, BC-408, BC-412, BC-416 Premium Plastic Scintillators. www.detectors.saint-gobain.com
16. Carcia PF, McLean RS, Reilly MH, Groner MD, George SM (2006) Appl Phys Lett 89:031915
17. Bläckberg L, Fay A, Jogi I, Biegalski S, Boman M, Elmgren K, Fritioff T, Johansson A, Mårtensson L, Nielsen F, Ringbom A, Rooth M, Sjöstrand H, Klintenberg M (2011) Nucl Instr Meth Phys Res A 656:84
18. Zaitseva N, Carman L, Glenn A, Newby J, Faust M, Hamel S, Cherepy N, Payne S (2011) J Crystal Growth 314:163